14. Ojemann GA. Cortical organization of language. *J Neurosci* 1991;11:2281–2287.
15. McCarthy G, Allison T, Spencer DD. Localization of the face area of human sensorimotor cortex by intracranial recording of somatosensory evoked potentials. *J Neurosurg* 1993;79:874–884.
16. King RB, Shell GR. Cortical localization and monitoring during cerebral operations. *J Neurosurg* 1987;67:210–219.
17. Herscovitch P, Markham J, Raichle ME. Brain blood flow measured with intravenous $H_2^{15}O$. I. Theory and error analysis. *J Nucl Med* 1983;24:782–789.
18. Raichle ME, Martin WRW, Herscovitch P, Mintun MA, Markham J. Brain blood flow measured with intravenous $H_2^{15}O$. II. Implementation and validation. *J Nucl Med* 1983;24:790–798.
19. Colebatch JG, Deiber M, Passingham RE, Friston KJ, Frackowiak SJ. Regional cerebral blood flow during voluntary arm and hand movement in human subjects. *J Neurophysiol* 1991;65:1392–1401.
20. Ohyama M, Senda M, Kitamura S, Ishii K, Mishina M, Terashi A. Role of nondominant hemisphere and undamaged area during word repetition in poststroke aphasics. A PET activation study. *Stroke* 1996;27:897–903.
21. Petersen SE, Fox PT, Posner MI, Mintun M, Raichle ME. Positron emission tomographic studies of the cortical anatomy of single-word processing. *Nature* 1988;331:585–589.
22. Fox PT, Mintun MA, Reiman EM, Raichle ME. Enhanced detection of focal brain responses using intersubject averaging and change-distribution analysis of subtracted PET images. *J Cereb Blood Flow Metab* 1988;8:642–653.
23. Senda M, Kanno I, Yonekura Y, et al. Comparison of anatomical standardization methods regarding the sensori-motor foci localization and between-subject variation in $H_2^{15}O$ PET activation, a three-center collaboration study. *Ann Nucl Med* 1994;8:201–207.
24. Senda M. Mapping cortical functions using PET activation technique. In: Sugishita M, ed. *New horizons in neuropsychology.* Amsterdam, The Netherlands: Elsevier Science; 1994:23–34.
25. Uemura K, Toyama H, Kimura Y, Nishina M, Senda M, Uchiyama A. Edge enhancing filter using modified fractal dimension for automatic edge detection of brain MRI. *J Cereb Blood Flow Metab* 1995;15:S605.
26. Rumeau C, Tzourio N, Murayama N, et al. Location of hand function in the sensorimotor cortex: MR and functional correlation. *AJNR: Am J Neuroradiol* 1994;15:567–572.

27. Grafton ST, Woods RP, Mazziotta JC, Phelps ME. Somatotopic mapping of the primary motor cortex in humans: activation studies with cerebral blood flow and positron emission tomography. *J Neurophys* 1991;66:735–743.
28. Rumsey JM, Andreason P, Zametkin AJ, et al. Failure to activate the left temporoparietal cortex in dyslexia. An ^{15}O positron emission tomographic study. *Arch Neurol* 1992;49:527–534.
29. Binder JR, Rao SM, Hammeke TA, et al. Lateralized human brain language systems demonstrated by task subtraction functional magnetic resonance imaging. *Arch Neurol* 1995;52:593–601.
30. Demb JB, Desmond JE, Wagner AD, Vaidya CJ, Glover GH, Gabrieli JD. Semantic encoding and retrieval in the left inferior prefrontal cortex: a functional MRI study of task difficulty and process specificity. *J Neurosci* 1995;5:5870–5878.
31. McCarthy G, Blamire AM, Rothman DL, Gruetter R, Shulman RG. Echo-planar magnetic resonance imaging studies of frontal cortex activation during word generation in humans. *Proc Natl Acad Sci USA* 1993;90:4952–4956.
32. Sakai K, Watanabe E, Onodera Y, et al. Functional mapping of the human somatosensory cortex with echo-planar MRI. *Magnet Res Med* 1995;33:736–743.
33. Villringer A, Dirnagl U. Coupling of brain activity and cerebral blood flow: basis of functional neuroimaging. *Cerebrovasc Brain Met Rev* 1995;7:240–276.
34. Ishiwata K, Kubota K, Murakami M, et al. Re-evaluation of amino acid PET studies: can the protein synthesis rates in brain and tumor tissues be measured in vivo? *J Nucl Med* 1993;34:1936–1943.
35. Derlon JM, Bourdet C, Bustany P, et al. Carbon-11-L-methionine uptake in gliomas. *Neurosurgery* 1989;25:720–728.
36. Mineura K, Sasajima T, Suda Y, Kowada M, Shishido F, Uemura K. Amino acid study of cerebral gliomas using positron emission tomography—analysis of (^{11}C-methyl)-L-methionine uptake index. *Neurol Med Chir Tokyo* 1990;30:997–1002.
37. Sato K, Kameyama M, Ishiwata K, Hatazawa J, Katakura R, Yoshimoto T. Dynamic study of methionine uptake in glioma using positron emission tomography. *Eur J Nucl Med* 1992;19:426–430.
38. Dierckx RA, Martin JJ, Dobbeleir A, Crols R, Neetens I, De Deyn PP. Sensitivity and specificity of ^{201}Tl single-photon emission tomography in the functional detection and differential diagnosis of brain tumors. *Eur J Nucl Med* 1994;21:621–633.
39. Golfinos JG, Fitzpatrick BC, Smith LR, Spetzler RF. Clinical use of a framelessstereotactic arm: results of 325 cases. *J Neurosurg* 1995;83:197–205.

Graphical Analysis of 6-Fluoro-L-Dopa Trapping: Effect of Inhibition of Catechol-O-Methyltransferase

J.E. Holden, D. Doudet, C.J. Endres, G.L-Y. Chan, K.S. Morrison, F.J.G. Vingerhoets, B.J. Snow, B.D. Pate, V. Sossi, K.R. Buckley and T.J. Ruth

Department of Medical Physics, University of Wisconsin, Madison, Wisconsin; and Neurodegenerative Disorders Centre and TRIUMF, University of British Columbia, Vancouver, British Columbia

Graphical methods to analyze tracer time-course data allow reliable quantitation of the rate of incorporation of tracer from plasma into a "trapped" kinetic component, even when the details of the kinetic model are unknown. Applications of the method over long time periods often expose the slow reversibility of the trapping process. In the extended graphical method, both trapping rate and a presumed first-order loss rate constant are estimated simultaneously from the time-course data. **Methods:** We applied the extended graphical method to 6-fluoro-L-dopa (6-FD), simultaneously estimating the rate of uptake (K_i) and the rate constant for loss from trapped component (k_{loss}) in a single fitting procedure. We applied this approach to study the effects of two catechol-O-methyl-transferase inhibitors on the kinetics of 6-FD in cynomolgus monkeys. **Results:** Inhibition of peripheral O-methylation with either inhibitor, confirmed by high-performance liquid chromatography analysis of labeled compounds in arterial plasma, had no significant effect on K_i, in agreement with previously reported studies. In contrast, tolcapone, a catechol-O-methyl-transferase inhibitor, having central effects in addition to peripheral effects at the dosage used, decreased k_{loss} by 40% from control values ($p < 0.002$), whereas nitecapone, which has no known central activity, had no significant effect. **Conclusion:** This method provides insight into the neurochemical basis for the kinetic behavior of 6-FD in both health and disease and may be used to define the action of centrally active drugs that influence the metabolism of dopamine.

Key Words: 6-fluoro-dopa; reversible trapping; extended graphical method; PET; COMT inhibition

J Nucl Med 1997; 38:1568–1574

After the early work of Garnett et al. (*1*), PET with the tracer 6-fluoro-L-dopa (6-FD), labeled with ^{18}F, became a recognized and validated technique for the assessment of nigrostriatal function (*2*). The 6-FD is taken up into the nigrostriatal nerve terminals and decarboxylated to 6-fluorodopamine (6-FDA) (Fig. 1). Like dopamine, 6-FDA cannot cross the blood–brain barrier and is trapped. In all data reduction approaches, this apparently irreversible accumulation of label in the striatum is clearly identified. In particular, application of the graphical method (*3*) to data collected in the first 2 hr following bolus administration of 6-FD invariably yields straight-line behavior, in keeping with such irreversible trapping. However, extension of the measurements beyond 2 hr shows that the assumption of

FIGURE 1. Simplified hypothetical model of the determinants of 6-FD and 3-O-MFD kinetics in the terminals of nigrostriatal neurons. 6-FD, 6-FDA and the metabolites of 6-FDA are all potential substrates of central COMT.

bolus injection of 6-FD, the radioactivity concentration reaches a maximum, and time-courses in the striatum become clearly differentiated from those in all other brain structures (Fig. 2). The difference between striatal and nonstriatal radioactivity concentrations remains a monotonically increasing function of time up to 2 hr after injection. This is due to the presence of a large excess of activity of L-aromatic amino acid decarboxylase in the terminals of dopaminergic fibers. 6-FD, upon reaching this cytosolar space, is thus rapidly decarboxylated to 6-FDA and possibly sequestered in the granular vesicles that protect monoamine neurotransmitters from degradation by catabolic enzymes (9). The 6-FDA that is not stored is subject to deamination by MAO. Stored 6-FDA is released into the synaptic cleft as part of both tonic and phasic DA release. It can then be reabsorbed into the presynaptic terminal and possibly be restored, but more probably metabolized by MAO; be directly metabolized by COMT; or diffused away from its source neuron to undergo metabolic destruction at another site.

Three major potential roles of COMT can be identified in this sequence. First, it can catalyze the O-methylation of 6-FD itself. Because this process would not be identifiable in the PET time-course data, this rate has been set to zero in the compartmental models applied to the kinetics of 6-FD (7,8). Second, COMT could O-methylate 6-FDA to 6-fluoro-3-methoxy-tyramine. Finally, COMT can O-methylate the acetic acid analog (6-fluoro-DOPAC) produced from 6-FDA by both intra- and extraneuronal MAO. These three effects would be reduced by the use of central inhibitors of COMT. A reduction of the first process would allow an increased fraction of 6-FD to be trapped as 6-FDA and presumably increase the uptake rate constant (K_i). Reduction of the two other effects would lead to a reduction of k_{loss}.

Review of the Graphical Approach

The basic principle of the graphical method (10) is that incorporation of a tracer into an irreversibly accumulating kinetic component can be reliably identified in the data, even if all of the intermediate reversible components of the tracer kinetics are not fully understood or accurately represented by a model. The original method was based on several assumptions. First, the tracer kinetics in a given measurement field of view should include processes that would irreversibly immobilize (trap) the tracer label in that field. Multiple immobilizing processes could not be distinguished, but their sum could still be reliably identified. Second, all other kinetic processes must be reversible. The condition of reversibility required for the graphical method to give accurate results states that the slowest component of the plasma time-course must be slower than the slowest tissue components. This can always be accomplished by programmed infusion, that is, intentionally introducing a constant component into the plasma time-course. If a bolus administration is used, it is important to confirm that the slowest component of the plasma time-course is, in fact, sufficiently slow. Patlak et al. (10) have shown that if these conditions are met and enough time has passed to allow the reversible processes to equilibrate with the slow component of the arterial input function, the time-course of tracer in tissue can be decomposed into two simple kinetic components. The first is proportional to the arterial input time-course and thus becomes constant in time when divided by that time-course. The other is proportional to the running time integral under the arterial time-course. Thus, the ratio of the tissue time-course C_i and the arterial time-course, C_p, can be described as:

irreversibility breaks down with the appearance of a progressive loss of signal. This loss implies the combined events of metabolism of 6-FDA by catechol-O-methyl transferase (COMT) and monoamine oxidase (MAO) and diffusion of the metabolites out of the trapping compartment. COMT is a major intracerebral metabolic enzyme of dopamine, and the loss of trapped tracer may therefore be affected by the central activity of COMT inhibitors in living subjects. The major effect of recently developed COMT inhibitors is believed to be the inhibition of breakdown of levodopa in the blood (4,5). The COMT inhibitor tolcapone (Ro 40-7592) has been shown to also inhibit central COMT activity in the rat (4,5). In contrast, nitecapone (Or 462) acts only peripherally. In this paper, we present a method to identify and quantify the reversibility of the trapping process (k_{loss}) in 6-FD kinetics by an extension of the graphical method. We apply that method in untreated monkeys and in monkeys treated either with tolcapone or nitecapone. We explored the hypothesis that tolcapone, but not nitecapone, inhibits central COMT activity in living nonhuman primates and therefore decreases k_{loss}.

Role of Central COMT

Figure 1 presents a simplified model of the kinetics of the tracer compound 6-FD when its extracerebral decarboxylation has been suppressed by carbidopa (6). Both 6-FD and its COMT metabolite 3-O-methyl-6-fluoro-L-dopa (3-O-MFD) are transported into brain by the neutral amino acid transport system. This plasma-to-brain transfer is quite homogeneous throughout all brain gray matter structures, with rate constants estimated to be about 0.05 ml/g · min (7,8). Between 10 and 15 min after
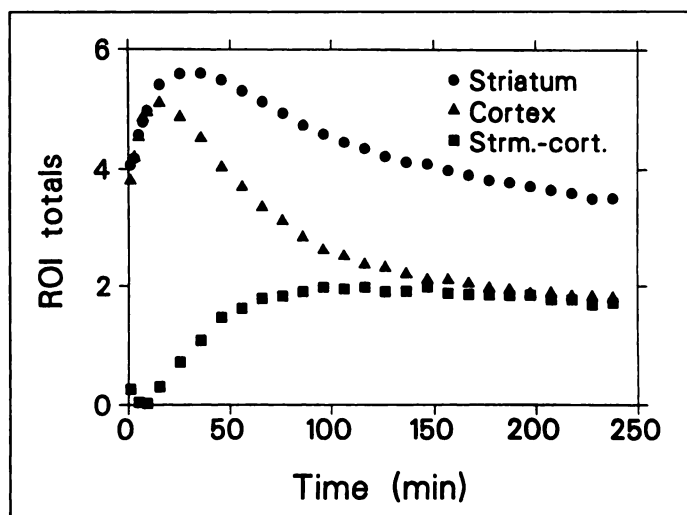
FIGURE 2. Characteristic radioactivity concentration time-courses in striatum and occipital cortex and their difference over a 4-hr period after bolus injection of 6-FD in cynomolgus monkey. Strm. = striatum; cort. = cortex.

$$\frac{C_i(t)}{C_p(t)} = V + K_i\frac{\int_0^t C_p(t)\,dt}{C_p(t)} = V + K_i\theta(t), \qquad \text{Eq. 1}$$

where V is a constant and the coefficient K_i is the desired rate of uptake from plasma into the irreversibly accumulating component. The variable $\theta(t)$ is defined by this equation to be the time integral of the plasma input function to time t, divided by the value of the input function at that time. It has dimensionality time and has been variously called integral time, modified time or stretch time. The ratio of tissue concentration to plasma concentration of a trapped tracer plotted versus stretch time thus eventually should take on a straight-line behavior, with a slope equal to the desired uptake rate. In the application of the graphical method to 6-FD uptake (3), the time-course, C_i, in the target striatal tissue is computed from region of interest (ROI) data. All components, reversible or irreversible, must arise only from 6-FD itself entering the brain. This last condition may be confounded by the presence of the labeled metabolite 3-O-MFD in both plasma and brain (Fig. 1). In the original application of the graphical method to 6-FD data, the assumption was made that the kinetics of 3-O-MFD are identical in all brain regions and, thus, that the subtraction of the time-course in some nonstriatal tissue from that in striatal tissue would leave a different time-course with negligible contributions from 3-O-MFD. If the trapping process is not truly irreversible, the pattern of $C_i(t)/C_p(t)$ versus $\theta(t)$ no longer follows a straight line; rather, the slope progressively decreases as time passes (Fig. 3, open squares). The curved behavior of the pattern can be interpreted as the ordinate increasing too slowly; clearly, the straight-line behavior would be restored if somehow we could add the lost tracer back into C_i at each time point. It is more useful, however, to interpret the curvature in terms of the abscissa increasing too rapidly. It has been shown (11) that if the loss of the trapped component is well described by a first-order process with rate constant k_{loss}, then the original formalism expressed in Equation 1 is modified only in the definition of $\theta(t)$:

$$\theta(t) = \frac{\int_0^t C_p(t') \exp\left(-k_{loss}(t-t')\right)dt'}{C_p(t)}. \qquad \text{Eq. 2}$$

Straight-line behavior would be restored, in principle, if the loss rate constant k_{loss} used to estimate the values of $\theta(t)$ were equal to the actual loss rate during data acquisition. Use of this

alternative estimate of $\theta(t)$ does not alter the ordinate values of the data points. If the time-course $C_p(t)$ decreases with time, then the abscissa values are all reduced, with the largest values undergoing the largest reduction. The application of this principle to 6-FD data is described below.

MATERIALS AND METHODS

Subjects and Pharmaceutical Dosages

Seven juvenile to young adult male cynomolgus monkeys (*Macaca fascicularis*) weighing 3–7.5 kg were studied over an 18-mo period. Five studies were performed with no pharmacological intervention (control). Seven studies were performed after pretreatment with tolcapone (29.8 ± 6.9 mg/kg i.p.), and six were performed after pretreatment with nitecapone (20.8 ± 3.0 mg/kg i.p.). Both COMT inhibitors were diluted in 1–1.5 ml of DMSO before i.p. administration. Pretreatment was performed at least 1 hr before administration of the 6-FD tracer (110 Mbq). Carbidopa (6) (2 mg/kg) was administered intraperitoneally 1 hr before the start of the study in all cases.

PET Image and Plasma Time-Course Data Acquisition

Subjects were fasted overnight, and a ketamine/pentobarbitol preanesthetic was followed by isoflurane anesthesia for the duration of the experiment. Studies were performed on the UBC/TRIUMF PETT VI positron camera (12). This camera permits simultaneous acquisition of seven axial planes, with a center-to-center separation of 14.4 mm, an average in-plane resolution of 9.2 mm FWHM and an axial resolution of 11 mm FWHM. Fluorine-18–6-FD (13) was administered as a bolus, and a 4-hr dynamic image sequence (twenty-four 10-min time frames) was started simultaneously. By moving the bed position, four interleaved sets of image planes were acquired at the end of the dynamic sequence to provide an axial sampling interval of 4 mm over the striatal region. Arterial blood samples were acquired at intervals (eight samples drawn continuously in the 1st min, followed by samples at 1.5, 2, 3, 4, 5, 7.5, 10, 20, 30, 60, 90, 120, 180 and 240 min) throughout the dynamic imaging sequence and used to determine the time-course of total radioactivity concentration in plasma. The labeled compounds in plasma were identified and quantified at six time points (10, 30, 60, 120, 180 and 240 min) using high-performance liquid chromatography analysis (14). The fractions attributed to 6-FD were fitted to the sum of two declining exponential functions. Estimates of the statistical precisions of the measured fractions were made at each time point and used to weight the fitting process. The total radioactivity concentration was then multiplied by the fitted 6-FD fraction, determined at the time of each sample, to yield the 6-FD time-course.

Preparation of the Image Data for Graphical Analysis

The six frames acquired during the second hour were summed into a single image set and used for the manual placement of elliptical ROIs. Regions encompassed left and right striata and occipital cortices. These ROIs were applied to the whole study, and the sums of all region pixel values were computed. The specific striatal time course on each side (left and right) was computed by subtracting the total signal in an area-matched cortical region from the total striatal time-courses. Factors to correct for interstudy variation in axial positioning were determined by a method similar to our previously reported approaches in human subjects (15). The axial distribution of the striatal ROI values measured in the interleaved datasets acquired after the dynamic study was fitted to a Gaussian function with the FWHM fixed at the previously determined value of 17 mm. A correction factor was calculated as the ratio between the peak of the fitted curve and the value corresponding to the axial position where the dynamic sequence was acquired. Specific striatal ROI values in the dynamic time-
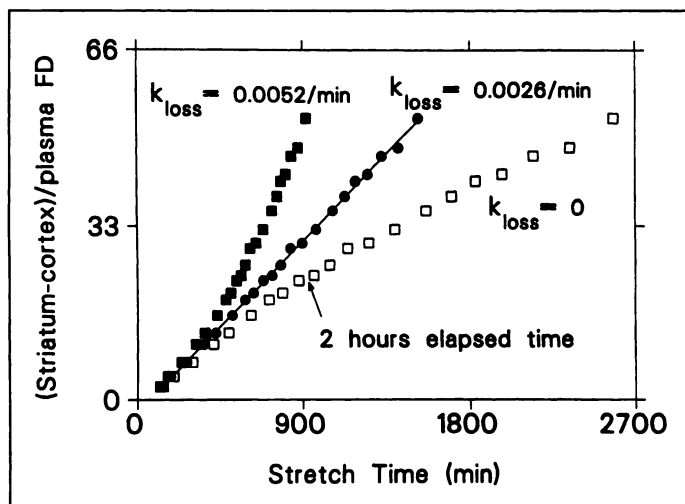
FIGURE 3. Evaluation of k_{loss} by the extended graphical method. Open squares, conventional graphical method applied to the entire 4-hr dataset; negative (concave down) curvature of the points at later times is clearly evident. Filled circles, extended graphical method with k_{loss} value determined to give optimal straight line behavior over the entire period. Filled squares, k_{loss} value twice the optimal value. The curvature is now positive (concave up).

course data were thus adjusted to the level that would have been observed if the striatum had been exactly centered in an axial plane. The mean factor for 18 studies was 1.07 (range, 1.0–1.25). The time-course values were then scaled by a fixed factor based on the assumed Gaussian axial distribution and the known voxel volume to convert the specific ROI data to values reflecting the total quantity of radioactivity in the total striatum. The corrected, scaled left and right specific striatal time-courses were then averaged to provide a single specific striatal time-course for each study. These time-courses were analyzed by conventional graphical analysis (3) and for k_{loss} as follows.

Evaluation of k_{loss}

In our approach to the model-independent evaluation of k_{loss}, Equation 2 is executed at 40 different values of k_{loss}, ranging from 0 to 0.008 min^{-1}. Each execution produces a set of ordered pairs (Fig. 3), and the pattern of C_i/C_p versus $\theta(t)$ is fitted to a second-order polynomial. For trial k_{loss} values smaller than the true one, the model estimation of the accumulation of trapped product is still exaggerated, and the curvature is still concave down (negative coefficient of the quadratic term in the second-order fit). For model k_{loss} values larger than the true one, the model estimate of the loss of accumulated trapped product is exaggerated, and the curvature is concave up (Fig. 3, solid squares). Straight-line behavior is attained at the value of k_{loss} at which the coefficient of the quadratic term changes sign, that is, passes through zero (Fig. 3, solid circles). The first pass of 40 different curvature estimates is used as a coarse determination; the process is then repeated over a smaller range of k_{loss} values centered around this coarse estimate, but with a correspondingly smaller step size. In this way, the k_{loss} value at which the curvature of the pattern of points changes sign can be determined to an arbitrary degree of precision. The mean squared discrepancy derived in an independent straight-line fit of the ordered pairs is also calculated at each k_{loss} value as an alternative optimization measure. This procedure is equivalent to the least-squares optimization of K_i and k_{loss} by Equations 1 and 2; the k_{loss} values determined from these two approaches agreed within a few percent of the their values in every case fitted to date.

The significance of group differences in k_{loss} was evaluated by the two-tailed, unpaired Student's t-test.

Methodological Studies

Particular methodological questions were also addressed by an extended analysis of the data. The effect of the range of fitting times was tested by repeating the estimation process in all datasets as the start and stop times of the fitting range were varied. The sensitivity to stop time was of particular interest. If the first-order assumption for the loss process were not valid, it would be possible for the loss rate to appear to accelerate as the study duration increased, that is, the apparent k_{loss} value would increase simply because study duration was increased. As peripheral COMT activity is suppressed, 6-FD in plasma falls more slowly, and the stretch time values corresponding to a given actual elapsed time postinjection are decreased accordingly. Thus effective study durations are shortened with peripheral COMT inhibition, and this in turn may result in a diminished apparent k_{loss} value. It was thus important to establish the effect of study duration (stop time) on the optimal k_{loss} value, particularly in the untreated group. The significance of the results of these tests is described below.

RESULTS

Plasma Metabolite Fractions

Characteristic time-courses of the plasma metabolite fractions determined by high-performance liquid chromatography over the 4-hr study duration are shown for the three study groups in Figure 4. The appearance of 3-O-MFD in plasma was nearly obliterated by tolcapone at the dose used, even out to 4 hr postinjection. This was accompanied by enhanced fractions of both the parent 6-FD and the conjugated metabolite, relative to the untreated (control) state. Pretreatment with nitecapone gave only partial suppression of 3-O-MFD production.

Graphical Analysis: Effects of COMT Inhibition

Conventional graphical analysis was used to fit the data acquired between 30 and 120 min postinjection. Good agreement between data and the model straight line was observed in all cases, and no significant differences in uptake rate values were observed among the study groups (Table 1). However, in no case did the extrapolation of the 2-hr best-fit straight line to later times correspond well to the later measured data. There was a strong suggestion of group differences in the patterns of the progressively increasing discrepancies between data and the extrapolated straight lines (Fig. 5).

The extended graphical method was used to fit the data acquired between 30 and 240 min postinjection. The rate of uptake from plasma into the trapped striatal component (K_i) and the rate constant for loss from that component (k_{loss}) were evaluated in each case. Good agreement between data and the model straight-line behavior was observed in all cases in all groups (Fig. 6).

Just as for the 2-hr graphical analysis, the uptake rate values were not significantly different in treated and untreated subjects (Table 1). However, the values for k_{loss} (Table 1), measured after pretreatment with tolcapone, were significantly decreased relative to those in both other groups (p < 0.002 versus untreated; p < 0.02 versus nitecapone). Values measured after pretreatment with nitecapone were not significantly different from those in the untreated group (p = 0.15). The discrepancies between the K_i values determined from 2 hr and those determined from 4 hr of data (Table 1) imply that the slope determined from 2 hr of data already suffers from the effects of k_{loss}, even though no curvature is evident in the data (Figs. 5 and 6).

FIGURE 4. Characteristic time-courses of labeled compounds in plasma expressed as fractions of the total radioactivity concentration. The three sets of curves are representative of the control, nitecapone and tolcapone groups. Open circles, 3-O-MFD; filled circles, 6-FD; open squares, sulfated conjugate; filled squares, 6-fluoro-DOPAC.
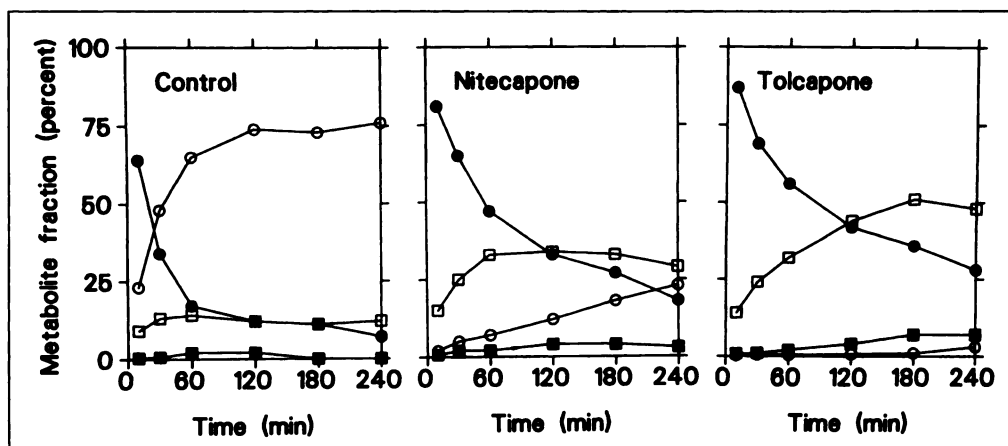
Methodological Studies

The fitted k_{loss} values showed a remarkable independence from the choice of fitting range start time (Fig. 7) in all three groups. Neither the value nor the variance of k_{loss} changed perceptibly as the start time of the fitting range was varied from 10 to 50 min postinjection, with the stop time held fixed at 240 min. As the final time of the fitting range varied from 2.5 to 4 hr, with the start time held fixed at 30 min, the primary effect seen was a decrease in variability as the fitting range was extended (Fig. 7). The mean value in the untreated group fell slightly, but not significantly, as the stop time was increased.

DISCUSSION

We have developed an approach for the identification and quantitation of the rate of reversibility of the trapping of 6-FD in striatal tissues. The method is based on the extended graphical method of Patlak and Blasberg (11). The curvature seen in the conventional graphical analysis of studies longer than 2 hr is interpreted as the slow loss of the trapped kinetic component by a first-order process; graphical analysis that includes this effect is performed at multiple values of the loss rate constant to identify the rate constant value that restores the straight-line behavior of the graphical analysis over the entire study duration. Extended graphical fits of eighteen 4-hr datasets acquired in cynomolgus monkeys consistently showed good agreement with the data; residuals at each time point were random. The uptake and loss parameter values thus exhaust the information available in the measured time-course data for the time period after equilibration of tissue with blood. The approach is different from alternative approaches based on compartmental models, primarily in the relative model independence of the estimation process. Because the loss rate constant has a value with order of magnitude 10^{-3} min^{-1}, the quality of the estimation process depends on the study duration. Our development project was performed with studies of 4-hr duration.

The method for estimation of the rate of reversibility sets requirements on the acquired data that are common to all applications of the graphical approach. In particular, all components of the fitted C_i, whether trapped or reversible, must arise only from tracer that enters the brain as 6-FD. However, accumulating 3-O-MFD is known to mimic the trapped component of 6-FD in striatum (16), and whole-body clearance processes would give it a high apparent value of k_{loss}. Slight differences between the kinetics of 3-O-MFD in the striatum and in the subtracted reference tissue (17,18) may result in a positive 3-O-MFD residue in striatum, in turn resulting in increased apparent values of both K_i and k_{loss} in the presence of high levels of 3-O-MFD in plasma. However, despite large changes in the levels of plasma 3-O-MFD with COMT inhibition, neither inhibitor changed the mean value of K_i determined by either the classical or the extended graphical methods. Thus, any incompletely canceled residue of 3-O-MFD in striatum is apparently small, and its influence on the fitted values of k_{loss} would not be expected to be significant.

The absence of change in K_i is in keeping with previous studies of the effects of peripheral inhibition of COMT on the kinetics of 6-FD (19,20). In that work as in this, the increase of striatal signal with peripheral COMT inhibition was exactly compensated by the increase in plasma 6-FD, leaving the mean K_i value unchanged. In addition, the absence of a change in uptake rate with high doses of the centrally active inhibitor tolcapone (4,5) suggests that central COMT does not interfere with the uptake of 6-FD to a significant degree.

In contrast with the unchanged K_i, the rate constant associated with the slow reversibility of the trapping process (k_{loss}) was reduced by 40% after pretreatment with tolcapone, whereas nitecapone did not alter it. These results are in keeping with the central activity unique to tolcapone, and they suggest that the observed prolongation of 6-FD trapping with tolcapone reflects the inhibition of 6-FDA metabolism in striatum (Fig. 1). This effect represents an increase of the mean life of the trapped component after 6-FD injection from 5.4 hr in the control group to 8.8 hr following tolcapone treatment. Such an effect may provide clinical benefit to patients with Parkinson's disease, both by preserving dopamine and by preventing wide fluctuations of synaptic dopamine levels. However, our results should be tempered by the fact that the dosage of tolcapone used in our study was around 6 times that prescribed in human treatment. Furthermore, the increased striatal dwell time may be due to the preservation of 6-fluoro-DOPAC as well as 6-FDA; the oxidation of 6-FDA to 6-fluoro-DOPAC and the subsequent elimination of this product by pathways that do not involve O-methylation almost certainly accounts for the failure of COMT inhibition to eliminate the loss rate completely.

TABLE 1
Graphical Method Results

Treatment	n	K_i (2 hr) (ml/min · str)	K_i (4 hr) (ml/min · str)	k_{loss} (4 hr) (min^{-1})
Untreated	5	0.027 ± 0.004	0.038 ± 0.006	0.0031 ± 0.0002
Nitecapone	7	0.029 ± 0.003	0.039 ± 0.005	0.0026 ± 0.0002
Tolcapone	6	0.030 ± 0.003	0.038 ± 0.004	0.0019 ± 0.0002*

Data are expressed as mean ± s.e.
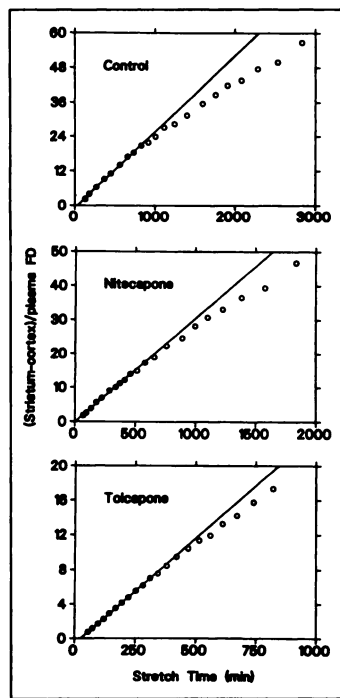*p < 0.002 vs. untreated; p < 0.02 vs. nitecapone.

FIGURE 5. Representative results of conventional graphical analysis. Graphical analysis was performed on the data collected in the first 2 hr (filled circles). The best-fit straight line was extrapolated over the remaining 2 hr and plotted along with the remaining data points (open circles).
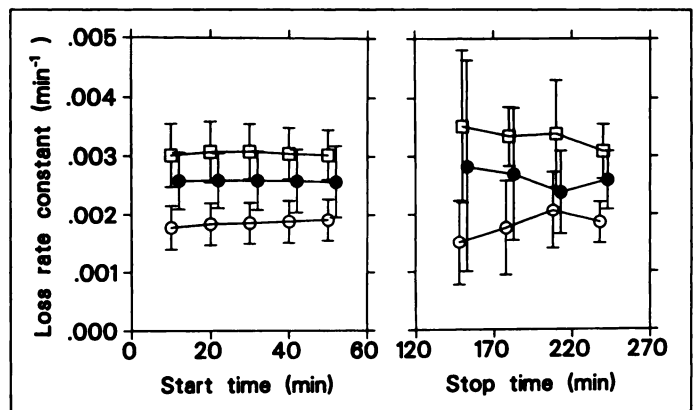

FIGURE 7. Effects of the fitting time range on the values and variability of k_{loss}. Left, start time varied with stop time fixed at 240 min. Right, stop time varied with start time fixed at 30 min. Open squares, control; filled circles, nitecapone; open circles, tolcapone. Points are offset slightly for clarity.

progressively increasing apparent loss rate as stretch times are extended to higher values.

CONCLUSION

The method reported here provides model-independent estimates of the rate of reversibility of the trapping of 6-FD in striatum. Application of this approach to 6-FD studies performed while the pharmacology of the dopamine system is intentionally altered by controlled interventions provides new insight into the physiological and neurochemical determinants of 6-FD kinetics.

ACKNOWLEDGMENTS

The mean k_{loss} value and its variability within each group were shown to be nearly independent of the fitting range start time over a wide range, as the corresponding stop time was held fixed at 4 hr. Thus, the 30- or 40-min start time conventionally used to assure stability of the derived K_i value should also assure the stability of the k_{loss} value. A similar test of the effects of stop time as start time was held fixed at 30 min yielded two results. First, the variability of the fitted k_{loss} values within each group decreased as stop time was increased; although the differences between groups also declined slightly at the same time, the most significant group differences were observed at the maximum stop time of 4 hr. Second, the systematics of the mean values of k_{loss} as stop time was increased indicated that the group differences reported here cannot be explained by a

FIGURE 6. Representative results of extended graphical analysis of the same three cases shown in Figure 5. The K_i values shown are those estimated simultaneously with k_{loss}.

REFERENCES

1. Garnett ES, Firnau G, Nahmias C. Dopamine visualized in the basal ganglia of living man. Nature 1983;305:137–138.
2. Vingerhoets FJG, Snow BJ, Schulzer M, et al. Reproducibility of fluorine-18–6-fluorodopa PET in normal human subjects. J Nucl Med 1994;35:18–24.
3. Martin WRW, Palmer MR, Patlak CS, Calne DB. Nigrostriatal function in humans studied with PET. Ann Neurol 1989;26:535–542.
4. Zurcher G, Dingemanse J, DaPrada M. Ro 40–7592, a potent inhibitor of extracerebral and brain catechol-O-methyltransferase: preclinical and clinical findings. In: Agnoli A, Campanella G, eds. New developments in therapy of Parkinson's disease. Rome: John Libbey; 1991:37–43.
5. DaPrada M, Zurcher G, Kettler R, Colzi A. New therapeutic strategies in Parkinson's disease: inhibition of MAO-B by Ro 19–6327 and of COMT by Ro 40–7592. In: Bernardi G, ed. The basal ganglia III. New York: Plenum Press; 1990:723–731.
6. Melega WP, Hoffman JM, Luxen A, et al. The effects of carbidopa on the metabolism of 6-[18F]fluoro-L-dopa in rats, monkeys and humans. Life Sci 1990;47:149–157.
7. Huang SC, Yu DC, Barrio JR, et al. Kinetics and modeling of L-6-[18F]fluoro-dopa in human PET studies. J Cereb Blood Flow Metab 1991;11:898–913.
8. Kuwabara H, Cumming P, Reith J, et al. Human striatal L-dopa decarboxylase activity estimated in vivo using 6-[18F]fluoro-L-dopa and PET: error analysis and application to normal subjects. J Cereb Blood Flow Metab 1993;13:43–56.
9. Pate BD, Snow BJ, Hewitt KA, et al. The reproducibility of striatal uptake data obtained with PET and fluorine-18-L-6-fluorodopa tracer in non-human primates. J Nucl Med 1991;32:1246–1251.
10. Patlak CS, Blasberg RG, Fenstermacher JD. Graphical evaluation of blood-to-brain transfer constants from multiple-time uptake data. J Cereb Blood Flow Metab 1983;3:1–7.
11. Patlak CS, Blasberg RG. Graphical evaluation of blood-to-brain transfer constants from multiple-time uptake data: Generalizations. J Cereb Blood Flow Metab 1985;5:584–590.
12. Evans B, Harrop R, Heywood D. Engineering developments on the UBC-TRIUMF modified PETT VI positron emission tomograph. IEEE Trans Nucl Sci 1983;NS-30:707–710.
13. Adam MJ, Jivan S. Synthesis and purification of L-6-[18F]-fluorodopa. Appl Radiat Isot 1988;39:1203–1206.
14. Chan GL-Y, Hewitt KA, Pate BD, Schofield P, Adam MJ, Ruth TJ. Routine determination of [18F]L-6-fluorodopa and its metabolites in blood plasma is essential for accurate positron emission tomography studies. Life Sci 1992;50:309–318.

15. Sossi V, Buckley KR, Snow BJ, et al. Recovery of the human striatal signal in a slice oriented positron emission tomograph. *J Nucl Med* 1993;34:481–487.
16. Holden JE, Pate BD, Adam MJ, Ruth TJ, Calne DB. Study of the effects of the labeled metabolite 3-O-methyl-6-fluorodopa on the interpretation of 6-fluorodopa kinetics measured with PET [Abstract]. *J Nucl Med* 1991;32:1007.
17. Doudet DJ, McLellan CA, Carson R, et al. Distribution and kinetics of 3-O-methyl-6-[18F]fluoro-L-dopa in the rhesus monkey brain. *J Cereb Blood Flow Metab* 1991;11:726–734.
18. Wahl L, Chirakal R, Firnau G, et al. The distribution and kinetics of [18F]6-fluoro-3-O-methyl-L-dopa in the human brain. *J Cereb Blood Flow Metab* 1994;14:664–670.
19. Laihinen A, Rinne JO, Rinne UK, et al. Fluorine-18-6-fluorodopa PET scanning in Parkinson's disease after selective COMT inhibition with nitecapone (OR-462). *Neurology* 1992;42:199–203.
20. Guttman M, Léger G, Reches A, et al. Administration of the new COMT inhibitor OR-611 increases striatal uptake of fluorodopa. *Mov Disord* 1993;8:298–304.

FIRST IMPRESSIONS
Technetium-99m-MDP Whole-Body Scintigraphy in Epidermoid Lung Tumor
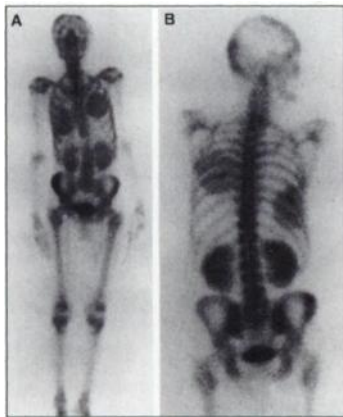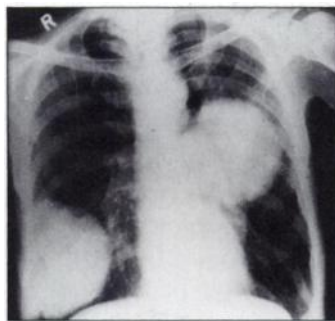

Figure 1.

Figure 2.

Figure 3.

PURPOSE
A 36-yr-old man with pain in the left iliac region was referred to nuclear medicine. Whole-body bone scintigraphy showed a round area of increased uptake in both hemithoraces and a focal area of increased uptake in the right iliac region (Fig. 1A,B). Chest radiography (Fig. 2) and magnetic resonance images (Fig. 3) showed mass lesions corresponding to these areas. Biopsy revealed that the patient had an epidermoid tumor of the lung.

TRACER
Technetium-99m-MDP, 740 MBq

ROUTE OF ADMINISTRATION
Intravenous

TIME AFTER INJECTION
3 hours

INSTRUMENTATION
Siemens Orbiter 7500, single-head detector with a LEAP collimator

CONTRIBUTORS
Seher Unal, Okan Falay and Sema Cantez, Istanbul Faculty of Medicine, Istanbul, Turkey